Hindawi
Advances in Materials Science and Engineering
Volume 2019, Article ID 6204302, 12 pages
https://doi.org/10.1155/2019/6204302

Research Article

Experimental Study on Constant-Amplitude Fatigue Performance of Weld Toe in Steel Tube of Welded Hollow Spherical Joints in Grid Structures

Jian-li Zhang, Hong-gang Lei, and Shi-hong Jin

College of Architecture and Civil Engineering, Taiyuan University of Technology, Taiyuan 030024, China

Correspondence should be addressed to Hong-gang Lei; lhgang168@126.com

Received 10 August 2018; Revised 17 December 2018; Accepted 8 January 2019; Published 22 January 2019

Academic Editor: Raffaele Sepe

The grid structure with welded hollow spherical joints (WHSJs) is widely used in industrial buildings with suspended cranes. Cyclic loadings generated by the suspended cranes could result in the fatigue failure of WHSJs. However, a corresponding fatigue design method has not been established. This paper presents an experimental study on the fatigue performance of the weld toe in the steel tube of WHSJs under axial force. Stress distribution on the joint's surface was obtained by the static load test. By using the MTS fatigue testing machine, a constant-amplitude fatigue test was performed on the full-scale joint specimens. Twenty effective test data were obtained and fitted to a fatigue *S-N* curve by the least squares method. The corresponding fatigue design method for allowable stress amplitude was established. The mechanism of fatigue failure at the joint was investigated through microscopic analysis using scanning electron microscopy. The results of this paper can be potentially used as a basis for revising specifications and to promote the practical application of grid structures with WHSJs.

1. Introduction

Welded hollow spherical joints (WHSJs) are widely used in the grid structures of industrial buildings, aircraft maintenance facilities, and public buildings. In 1965, these joints were first used in the project of Science and Technology Hall in Tianjin [1]. Since then, their applications were expanded, and they have become a major joint pattern used in spatial structures in China.

Many researchers have studied the performance of WHSJs subjected to a static load. For example, Han and Liu [2] and Wang and Luan [3] studied the ultimate bearing capacity of WHSJs under axial force and proposed a formula for the calculation of the ultimate bearing capacity. Dong et al. [4] studied the bearing capacity of WHSJs subject to combined axial force and bending moment and developed a practical calculation method. Sun [5] used the finite element analysis (FEA) to calculate the axial flexibility and flexural stiffness of WHSJs under an elastic state. Han et al. [6] proposed a practical formula for the initial stiffness of WHSJs and established a mechanical model to accurately simulate mechanical properties such as stiffness characteristics of the joints during loading and failure process. Liu et al. [7] experimentally and numerically studied the postfire residual mechanical behaviors of WHSJs. Lu et al. [8] studied the behaviors of eight WHSJs specimens subjected to standard fire exposure conditions, including the temperature distributions in the joints during the heating and cooling process and the mechanical behavior of the specimens after heating. Numerical methods were used by Zhao et al. [9] to study the effects of corrosion on the flexural stiffness and bending capacity of joints at different locations of WHSJs. However, there is limited research on the fatigue performance of WHSJs.

In industrial buildings, the suspended cranes are often installed on the grid structure to meet the requirements of production. The suspended cranes are more flexible and convenient to operate compared to traditional cranes (Figure 1). With the increase of economic growth and industrial demand, the level of cranes hanging on the grid

Figure 1: Grid structure with WHSJs with suspended cranes.

structure, the load size, and the usage frequency are increasing. Due to the self-weight of the suspended crane and dynamic load caused by the lifting weight, fatigue problems could occur in the grid structure [10, 11].

A load recorder was used by Xu and Cui [12] to record the random loads on cranes. According to the recorded data, lifting the crane once can produce several loading-unloading cycles. Based on this, they recommended that fatigue calculations should be carried out on the joints and their connected members which the suspended cranes directly acted on. The Technical Specification for Space Frame Structures [13] suggests that the fatigue calculation should be carried out when the number of cycles of stress change is greater than or equal to 5×10^4 in the grid structure which is subjected to a load from the suspended crane at a working level of A3 and above. The allowable stress amplitude and construction should be determined by experiments. However, for WHSJs, there are no corresponding fatigue design methods in related welding standards [14–17]. This hinders the proper design and the practical application of the grid structure in the industry. Thus, research studies on the fatigue performance of WHSJs have important engineering significance.

Fatigue failure of WHSJs may occur at the weld toe in the hollow sphere (location 1 in Figure 2) or in the steel tube (location 2 in Figure 2) on the sphere-tube junction. Fatigue failure at the weld toe in the hollow sphere has been studied by some researchers. For example, Lei [18] obtained the fatigue *S-N* curves by conducting fatigue tests on 15 full-scale WHSJs with four specifications. Based on the thin shell theory, the calculation formula of the hot-spot stress concentration factors at the weld toe in the hollow sphere was established. Yan [19] carried out fatigue tests of 29 full-scale WHSJs, obtained the fatigue *S-N* curves of weld toe in the hollow sphere, and established a practical fatigue design formula based on the nominal stress amplitude and hot-spot stress amplitude at the spherical surface of the joints.

However, there is little research on the fatigue performance of the weld toe in the steel tube. This motivates us to conduct experimental studies to understand the fatigue performance of weld toe in the steel tube.

2. Description of Specimens and Tests

2.1. Specimen Design. Twenty-two test specimens with two variations in dimensions were designed according to Technical Specification for Space Frame Structures (JGJ7-2010) and the general requirements of grid structure in engineering. The details are shown in Figure 3. The steel tube is a high-frequency welded tube, and the hollow sphere is not stiffened, which satisfies the requirements of JG/T11-2009 [20]. The end of the steel tube is connected to the hollow sphere using manual electric arc welding. The quality of the weld meets the requirements of JGJ7-2010.

The specimen ID (Group 1 and Group 2) and geometric parameters are shown in Table 1. D and T, respectively, represent the outside diameter and thickness of the hollow sphere; d and t, respectively, represent the outside diameter and the wall thickness of the steel tube; L indicates the length of the steel tube.

The materials used for the steel tube and the hollow sphere are Q235 B. The base material of the hollow sphere has a yield stress of 267 MPa and an ultimate stress of 395 MPa. The yield stress and ultimate stress of $Ø48 \times 3.5$ steel tubes are 284 MPa and 424 MPa, respectively; the yield stress and ultimate stress of $Ø60 \times 3.5$ steel tubes are 290 MPa and 472 MPa, respectively.

2.2. Test Scheme

2.2.1. Static Load Test. Each group of specimens had one specimen statically tested: Specimen 1 from Group 1 and Specimen 2 from Group 2. They were both subjected to axial tension in the tests. The test was divided into two stages. In the first stage, a static load test was conducted when the joint was under an elastic state, and in the second stage, the static load was applied until the joint failed. The static load test in the elastic stage was conducted to obtain the stress distribution of the joint's surface, while the purpose of the second stage test was to verify whether the joint meets the requirements of static load design and to obtain the failure mode of the joint under the static load.

To obtain the stress distribution on the surface of the joint, the strain gauges were adhered to the key positions of the joint. The strain gauges were arranged as shown in Figure 4. The strain gauges labeled as P1 to P8 were arranged on the tube surface, and S1 to S6 were arranged on the spherical surface, as shown in Table 2. The weld toes in both the steel tube and hollow sphere on the sphere-tube junction were subjected to multiaxial stresses. P7 and P8 at the weld toe in the steel tube and S1 and S2 at the weld toe in the hollow sphere were both attached with biaxial strain gauges. One of the strain gauges was perpendicular to the weld, and the perpendicular strain $\varepsilon_{\perp}$ was measured. The other was parallel to the weld, and the parallel strain $\varepsilon_{\parallel}$ was measured.

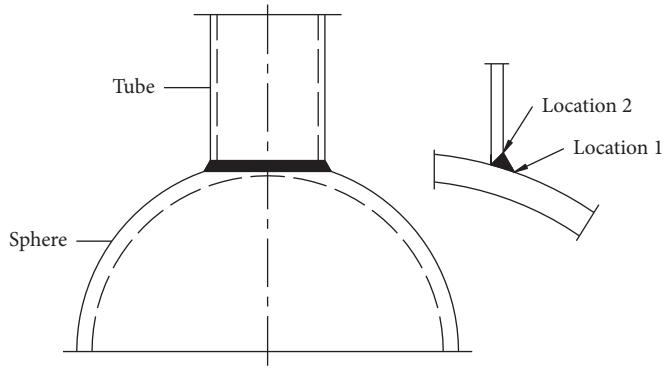

Figure 2: Fatigue failure positions of WHSJ.

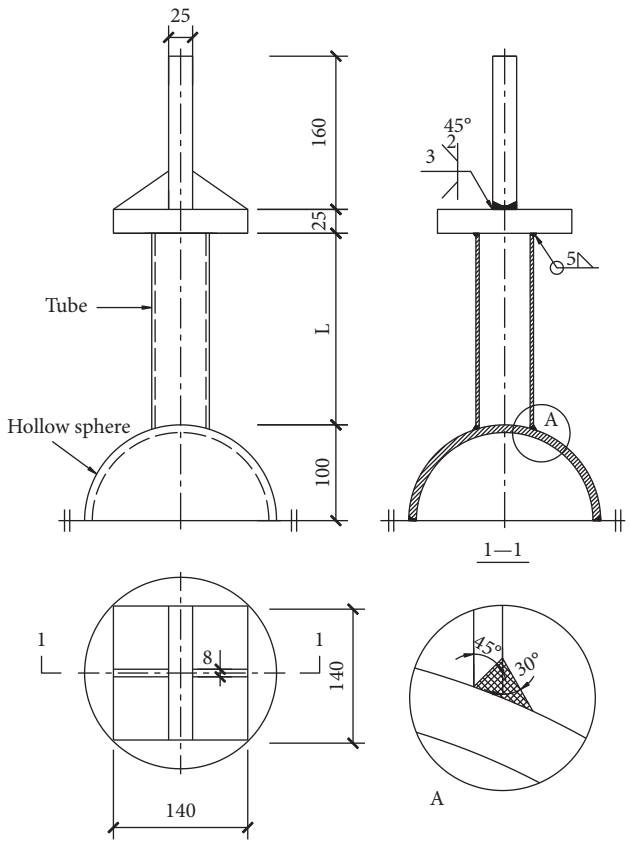

Figure 3: Specimen dimensions (unit: mm).

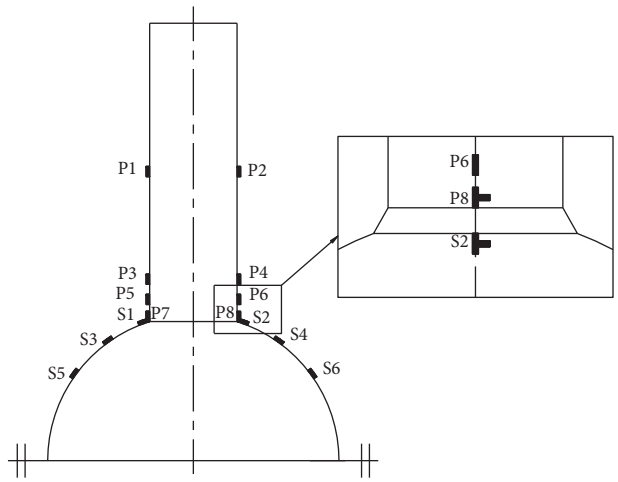

Figure 4: Typical gauge arrangement.

Table 1: Specimen ID and geometric parameters.

Specimen label	$D \times T$	$d \times t$	L
Group 1	200×8	48×3.5	180
Group 2	200×8	60×3.5	200

Table 2: Gauge position and its ID.

Measuring point	Gauge ID	Gauge position
Steel tube	P1, P2	Middle of steel tube
	P3, P4	30 mm from weld toe
	P5, P6	15 mm from weld toe
	P7, P8	Weld toe
Hollow sphere	S1, S2	Weld toe
	S3, S4	1/4 of exterior arc
	S5, S6	1/2 of exterior arc

Uniaxial strain gauges were attached at other positions to measure the perpendicular weld strain.

The test was carried out on a 200-ton tension machine, as shown in Figure 5. Preloading was carried out before formal loading to ensure that the strain gauges worked properly. The loading force was axial. All the measuring points were required to be in the elastic stage during the entire test. In such elastic field, the maximum load of Specimen 1 was 20 kN, and the maximum load of Specimen 2 was 30 kN. Multistage loadings were carried out, and each stage was held for three minutes. When the maximum load was reached, the strain gauge was used to measure the strain. After the first stage of the test, multistage loadings were performed on the specimens until the test specimen broke.

2.2.2. Fatigue Test. The constant-amplitude fatigue tests were performed on the MTS Landmark 370.50 fatigue testing machine, which is a fully digital servohydraulic fatigue test machine (Figure 6). The machine performs fatigue

Figure 5: Tension machine for the static load test.

Figure 6: MTS Landmark 370.50 for the fatigue test.

loads with different wave types, such as sine wave, square wave, triangular wave, and custom waveform. The load range that can be applied is ±500 kN, and the loading cycle frequency is up to 100 Hz.

The stress of some bottom chords significantly increases and the stress of some webs changes from tensile stress to compressive stress when suspended cranes act on the grid structure with WHSJs. Therefore, two stress ratios were used in this test. Specimens in Group 1 had a stress ratio of 0, while specimens in Group 2 had a stress ratio of 0.4. All fatigue tests were carried out at room temperature with a loading frequency of 10 Hz. The loading curve was a sine curve.

The surface of the fatigue fracture was examined by scanning electron microscopy after the fatigue test. Subsequently, the crack initiation location and its propagation direction could be analyzed and determined. The mechanism of fatigue failure of the joint was then analyzed.

3. Test Results and Discussion

3.1. Results of the Static Load Test

3.1.1. Stress Distribution on the Surface of Joints. The generalized Hooke's law (equation (1)) was used to convert strains to stresses at weld toes that were in the multiaxial stress state, while the relationship between stresses and strains at other locations can be described using $\sigma = E\varepsilon$.

$$\sigma_{\perp} = \frac{E}{1-\nu^2}\left(\varepsilon_{\perp} + \nu\varepsilon_{\parallel}\right),$$
$$\sigma_{\parallel} = \frac{E}{1-\nu^2}\left(\varepsilon_{\parallel} + \nu\varepsilon_{\perp}\right), \quad (1)$$

where $\sigma_{\perp}$ and $\sigma_{\parallel}$, respectively, represent the stress in the direction perpendicular to the weld toe and the stress in the direction parallel to the weld toe. E represents the elastic Young's modulus, and its value is 2.06×10^5 MPa. The value of Poisson's ratio ν is 0.3. $\varepsilon_{\perp}$ and $\varepsilon_{\parallel}$, respectively, represent the perpendicular strain and the parallel strain at the weld toe.

Table 3 shows that the parallel stress and the perpendicular stress at the weld toe in the steel tube on the sphere-tube junction calculated by the above formula are tensile stresses. The surface of the weld toe was in a biaxial tensile stress state, and the parallel stress was about 1/2 of the perpendicular stress. For Specimen 1 (load 20 kN), the perpendicular stresses at the middle of the pipe were 44.08 MPa and 42.64 MPa, which were close to the nominal axial normal stress of 40.87 MPa; for Specimen 2 (load 30 kN), the perpendicular stresses at the middle of the pipe were 50.06 MPa and 48.41 MPa, which were also close to the nominal axial normal of 48.29 MPa. These indicated that the stress state in the middle of the steel tube was almost the uniaxial stress state. From the middle of the pipe to the weld toe, the perpendicular stress changed due to the change of the stress state, and near the weld toe, it increased rapidly due to the stress concentration.

The surface stress of the hollow sphere also reached the maximum at the weld toe (Table 3). The parallel stress and perpendicular stress at the weld toe in the hollow sphere are tensile stresses, and the parallel stress was approximately 1/2 of the perpendicular stress. The stress at the weld toe reached its maximum, while at positions distant from the weld toe, the stress rapidly dropped. For example, at 1/4 of the exterior arc of the hollow sphere, the stress was reduced to 1/10 of the stress in the middle of the steel tube. This indicates that the adjacent members have limited impact on the stress of WHSJ, and it is feasible to study the performance of WHSJs by using the specimen that is subjected to a uniaxial force.

Table 3: Calculated stresses at the measuring points.

Gauge ID	Specimen 1 (MPa)	Specimen 2 (MPa)
P1	44.08	50.06
P2	42.64	48.41
P3	44.29	50.47
P4	42.85	47.79
P5	37.90	39.14
P6	33.99	38.11
$P7_{\perp}$	73.75	83.67
$P7_{\parallel}$	37.78	39.93
$P8_{\perp}$	66.01	83.33
$P8_{\parallel}$	34.63	42.92
$S1_{\perp}$	70.45	70.72
$S1_{\parallel}$	36.38	37.28
$S2_{\perp}$	63.95	65.10
$S2_{\parallel}$	32.57	36.42
S3	3.09	7.62
S4	3.296	7.21
S5	7.00	10.3
S6	7.622	9.27

3.1.2. Failure Mode of the Joints under Static Load. After the first stage was completed, the static load was continuously applied until the specimen failed. The failure fractures were both located in the middle of the steel tube, as shown in Figure 7. This type of failure is a strength failure. It can be seen that the section of the steel tube was thinner than before and that necking occurred as well. The direction of fracture is 45° to the tube axis. The ultimate bearing capacity of the WHSJs is shown in Table 4. Static load design values for the hollow sphere were calculated by

$$N_S = \left(0.29 + 0.54\frac{d}{D}\right)\pi T\ d f, \tag{2}$$

where D is the outside diameter of the hollow sphere, d is the outside diameter of the steel tube, T is the wall thickness of the hollow sphere, and f is the design value of steel's tensile strength and its value is 215 MPa. Static load design values for the steel tube were calculated by $N_t = fA$, where f is 215 MPa and A represents the area of the steel tube. Table 4 shows that the specimens satisfy the requirements of Technical Specification for Space Frame Structures (JGJ7-2010).

3.2. Fatigue Test Results

3.2.1. Fatigue Failure Mode. The fatigue failure at both stress ratios occurred at the weld toe in the steel tube, as shown in Figures 8 and 9. Figure 8 shows the fatigue failure of the specimen with a stress ratio of 0.4 and stress amplitude of 99 MPa, which means $\sigma_{max} = 165$ MPa and $\sigma_{min} = 66$ MPa. The crack had a symmetrical shape. The center of the crack was the widest and was where the crack initiated, as shown in Figure 8(b). The crack then propagated to both sides along the weld toe. In the central area of the crack, the steel tube was penetrated by the crack, and the fracture surface was perpendicular to the axis of the steel tube. Both ends of the crack were offset from the weld toe and extended to the steel tube, as shown in Figures 8(a) and 8(c). Figure 9 shows the fatigue failure of the specimen with a stress ratio of 0 and stress amplitude of 170 MPa, which means $\sigma_{max} = 170$ MPa and $\sigma_{min} = 0$ MPa. The fatigue failure mode of the specimen with a stress ratio of 0 is similar to the fatigue failure mode of the specimen with a stress ratio of 0.4.

The measured stresses on specimens subjected to static loads show that the stress at the weld toe in the steel tube reached maximum and the fatigue failure of the specimen also initiated in that area. The perpendicular stress on the surface of the weld toe was approximately twice the parallel stress, and the center of the fracture was perpendicular to the tube axis. As the loading force increased, the specimen was subjected to eccentric tension rather than axial tension, and the section area of the steel tube reduced until it could not resist the static load. In the end, fast propagation occurred when the stress exceeded the strength. The final fracture surface was at an angle of 45° to the tube axis, and the crack finally entered the steel tube area.

3.2.2. Data Analysis for Fatigue Test. Twenty effective data were obtained from 20 full-scale WHSJs in the constant-amplitude fatigue test. Two of the ten specimens in Group 1 were not destroyed after more than two million cycles, and the remaining eight specimens failed within two million cycles. Two of the ten specimens in Group 2 were not destroyed after more than two million cycles, and the remaining eight specimens failed within two million cycles. The fatigue failure data obtained from the failed specimens were used in the statistical analysis. The stress amplitude $S = \sigma_{max} - \sigma_{min}$ and the cycle number N were used as parameters to statistically analyze the data from the fatigue test. The stress amplitude is the nominal stress amplitude, which is the difference between the maximum and minimum axial forces divided by the steel tube area. N is the number of fatigue load cycles when the crack at the weld toe in the steel tube extends to half the length of the circumference of the entire steel tube.

Figure 10 shows the S-N curve that was obtained through data regression using the fatigue test data of all the two groups within two million cycles. As shown in Figure 10, the regression equation fits the set of fatigue test data well (correlation coefficient r of 0.937).

Fatigue test data are often fitted to a linear model with double logarithmic coordinates, with $\lg N$ as the dependent variable and $\lg S$ as the independent variable. The correlation between $\lg N$ and $\lg S$ can be obtained by linear regression analysis with the least squares method, as shown in

$$\lg N = A + B \lg S \pm 2 \cdot s, \tag{3}$$

where A is the intercept of the fatigue curve and B is the slope of the fatigue curve; s is the statistical standard deviation of the test data.

The two groups of fatigue failure data were, respectively, fitted to the $\lg S$-$\lg N$ curve by the least squares method, as shown in Figure 11. The results show that the two fitting curves of the two groups of data are close, indicating that the stress ratio has limited impact on the fatigue strength, and

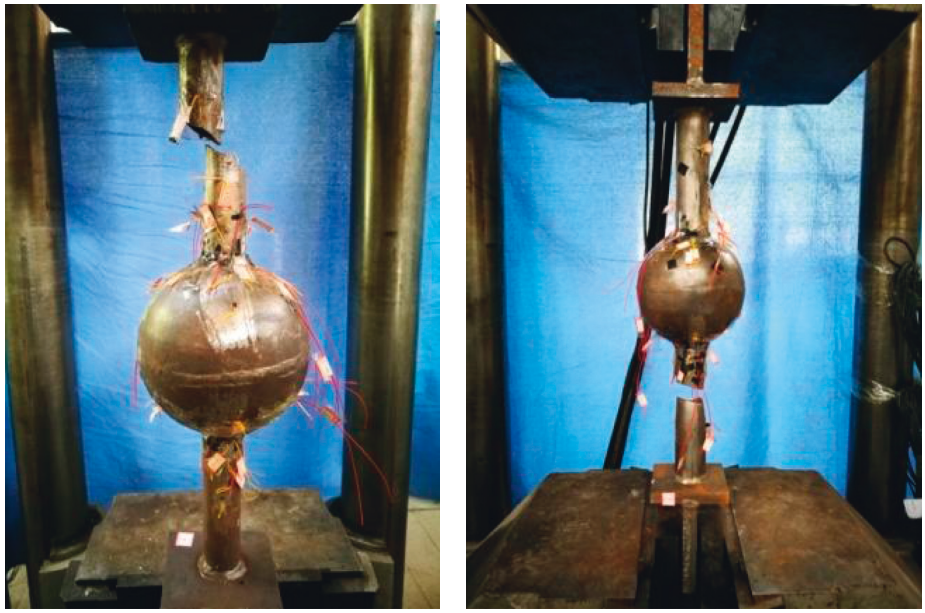

(a) (b)

Figure 7: Static load-induced failure mode. (a) Specimen 1. (b) Specimen 2.

Table 4: The design values and ultimate bearing capacity values of WHSJs.

Specimens	Static load design values for steel tube (kN)	Static load design values for hollow sphere (kN)	Ultimate bearing capacity of joints (kN)	Failure position
Specimen 1	105	109	219.95	Middle of tube
Specimen 2	134	147	293.22	Middle of tube

the stress amplitude is the main parameter which determines the fatigue life of WHSJs, at least in the range of the examined stress ratios.

All fatigue failure data were analyzed using the least squares method of statistical analysis to obtain a $\lg S$-$\lg N$ curve, as shown in Figure 12. The results in Figure 12 show that the measured data from this test have larger values than the mean value minus two standard deviations. The corresponding mean curve, mean-minus-two-standard-deviation curve and mean-plus-two-standard-deviation curve are expressed by $\lg N = 13.5639 - 3.8155 \lg S \pm 2 \times 0.1557$. The stress amplitude corresponding to the two million cycles on the curve of mean-minus-two-standard-deviation curve is 66.36 MPa. The fatigue test data fit to a normal distribution, with 95% of the data points falling within the mean plus or minus 1.96 standard deviation. This means that 66.36 MPa has a survival rate greater than 95%.

3.2.3. Fatigue Fracture Analysis. Fracture analysis is an important tool for investigating the fracture mode of a material or component. It can also provide the important information of crack initiation, crack propagation direction, and final fracture.

Figure 13(a) is a macroscopic fracture image of a specimen with a stress amplitude of 123 MPa and a stress ratio of 0.4. The fracture is divided into three regions: crack initiation zone, crack propagation zone, and fast fracture zone. The fatigue initiation zone is located at the center of the fracture, and the crack propagation zone is smooth as a result of the rubbing of both sides of the crack during the cyclic loads. The fast fracture zone is rough due to the rapid failure of the material. The fatigue initiation zone is magnified 45 times by means of a scanning electron microscope, as shown in Figure 13(b). It can be seen that the crack initiation occurred from the weld concavity where the surface welding defect occurs. By magnifying 10,000 times the position 1 mm away from the outer wall, it can be seen that the fatigue crack propagation zone is characterized by fatigue striations, as shown in Figure 13(c). The fatigue striations are parallel and slightly convex to the inside, indicating that the fatigue crack propagated from the outside to the inside. The position of 2 mm from the outer wall is magnified 500 times, as shown in Figure 13(d). It shows that the secondary crack is intermittently distributed on the fracture; it is deeper than that of the fatigue striations on the fracture, and the direction is perpendicular to the expansion direction. The position near the inner wall of the steel tube is magnified 300 times (Figure 13(e)). It shows that the surface fluctuation increases, which indicates that although the nominal stress is not large, the wall thickness of the steel tube decreases and the stress at the crack tip increases due to the crack's propagation. When this position is magnified 10000 times, as shown in Figure 13(f), the width of the fatigue

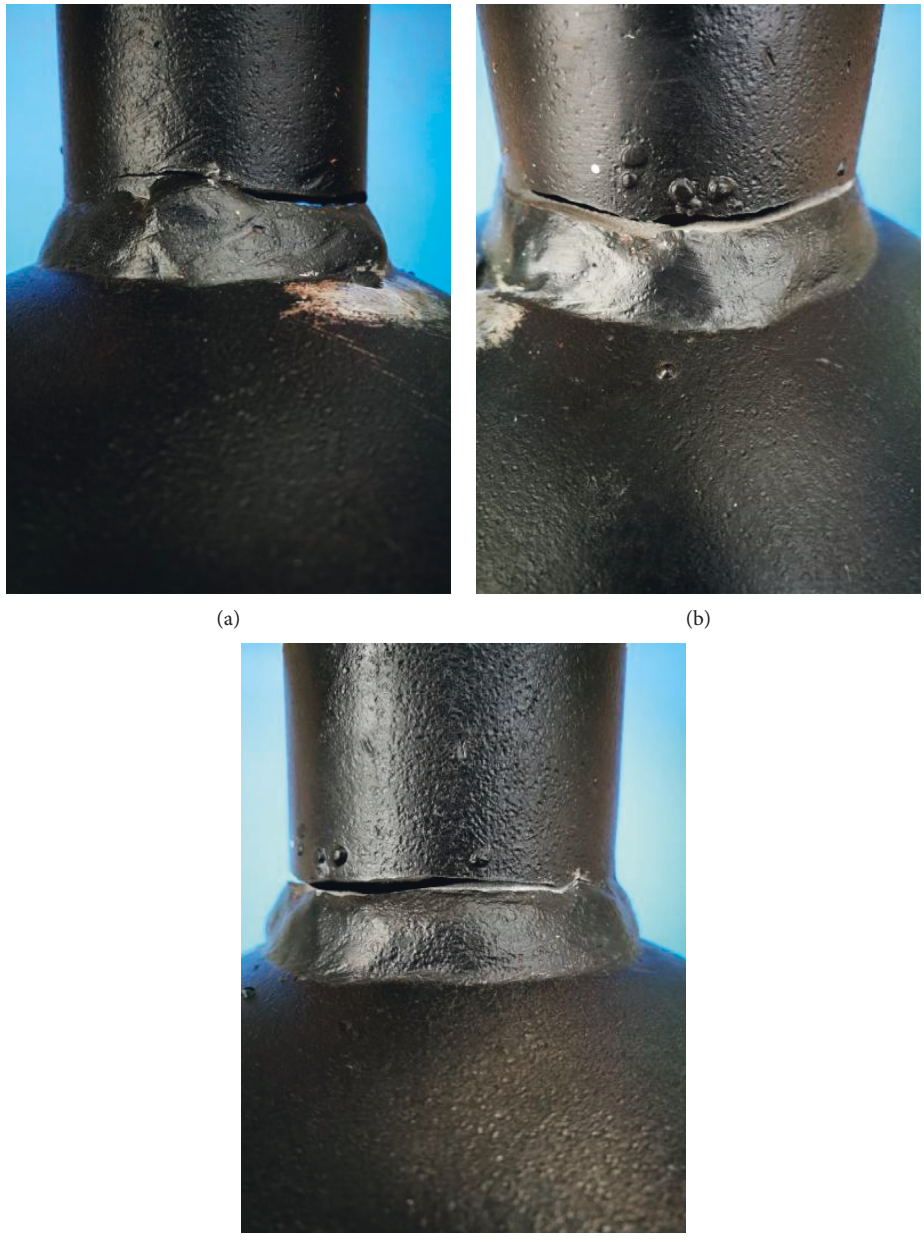

(a) (b)

(c)

Figure 8: Typical fatigue failure mode (stress amplitude = 99 MPa; stress ratio = 0.4). Left side (a), center (b), and right side (c) of the fracture.

striation and the spacing between fatigue striations increased, compared to Figure 13(c). In the center of the crack, the microscopic characteristics of the entire wall thickness of the steel tube are fatigue striations, and the fatigue crack penetrates the wall thickness.

Figure 14(a) is a macroscopic fracture image of a specimen with a stress amplitude of 155 MPa and a stress ratio of 0. The fracture has three regions of fatigue fracture: crack initiation zone, crack propagation zone, and fast fracture zone. Figure 14(b) is a microscopic image of the fracture with 45 times magnification. The crack initiation occurred from the weld concavity where the surface welding defect occurs. The fatigue crack propagated from the outside to the inside. Figure 14(c) is a microscopic image of the fatigue crack propagation zone with 5000 times magnification. The microscopic characteristics are fatigue striations. Figure 14(d) is a microscopic image of the fast fracture zone, characterized by dimples.

The fatigue failure of the specimen was located at the weld toe in the steel tube. The fatigue crack initiated from the surface of the steel tube and propagated from the outside to the inside until it penetrated through the steel tube wall. The fatigue failure of the specimen was caused mainly by the stress concentration at the weld toe in the steel tube. After analyzing the fracture of the specimen, it can be seen that, along the entire weld toe in the steel tube, the welding defects were more likely to become a fatigue initiation. The welding defects have a significant impact on the fatigue failure of the

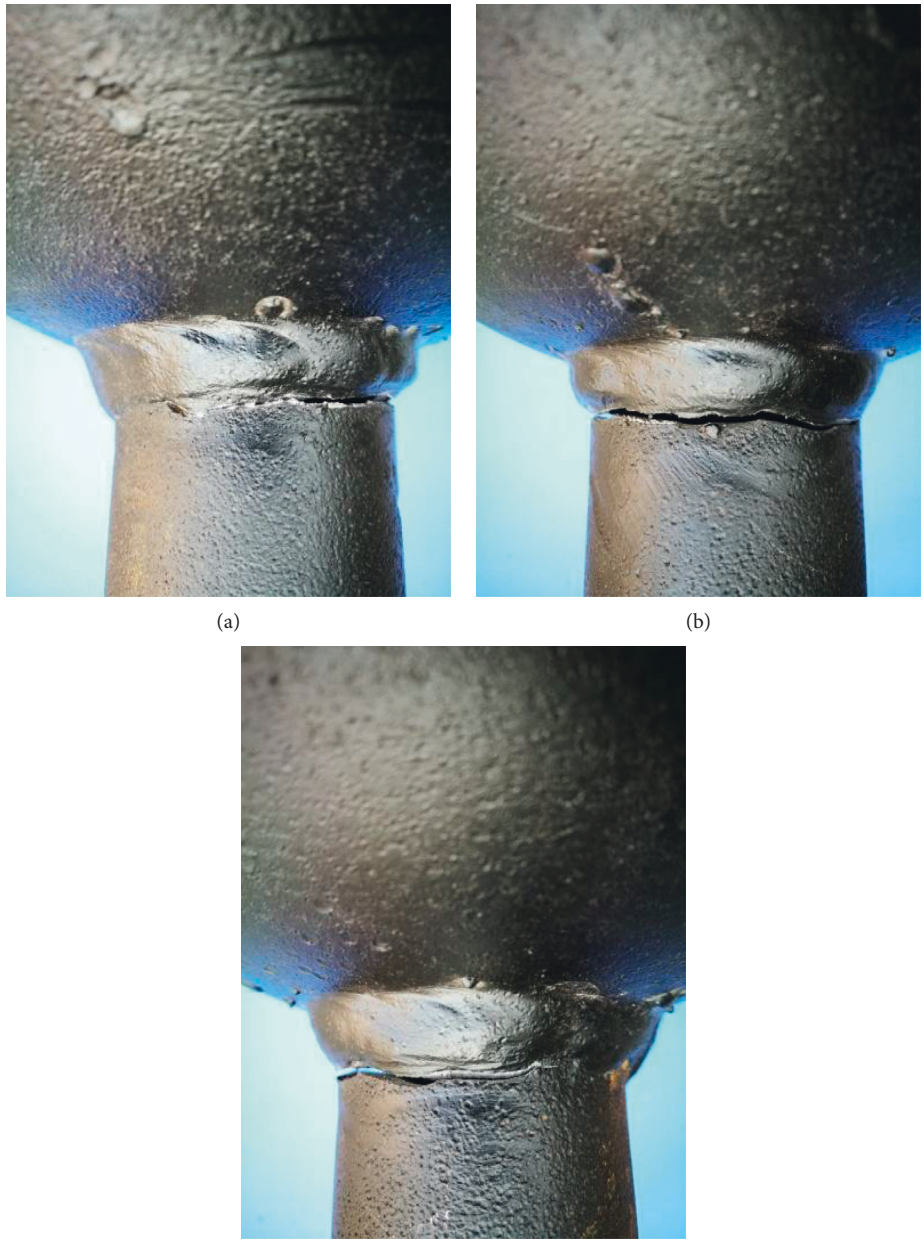

(a) (b) (c)

Figure 9: Typical fatigue failure mode (stress amplitude = 170 MPa; stress ratio = 0). Left side (a), center (b), and right side (c) of the crack.

joints, but have no significant effect on the joints that are subjected to a static load. The static-load induced specimen failure as the stress exceeded the strength during the loading. As the strength of the joint is greater than the strength of the steel tube, the failure under static load occurred at the middle of the steel tube.

4. Establishment of Fatigue Design Method

The fatigue calculation of the weld toe in the steel tube of WHSJs can be performed by the fatigue design method with the nominal stress amplitude as the parameter, as shown in

$$\Delta\sigma_{\text{nom}} \leq [\Delta\sigma], \tag{4}$$

where $\Delta\sigma_{\text{nom}}$ is the nominal stress amplitude of the steel tube (N/mm^2), $\Delta\sigma_{\text{nom}} = \Delta\sigma_{\max} - \Delta\sigma_{\min}$, $\Delta\sigma_{\max}$ is the maximum stress in the axial direction of the steel tube, and $\Delta\sigma_{\min}$ is the minimum stress in the axial direction of the steel tube; $[\Delta\sigma]$ is the allowable stress amplitude (N/mm^2) at the weld toe in the steel tube, which is given by

$$[\Delta\sigma] = \left(\frac{C}{N}\right)^{1/m}, \tag{5}$$

where C and m are constants, $m = 3.8155$ and $C = 1.789 \times 10^{13}$ and N is the number of cycles.

Equation (5) was derived by the mean-minus-two-standard-deviation $\lg S$-$\lg N$ curve $\lg N = 13.5639 - 3.8155 \lg$

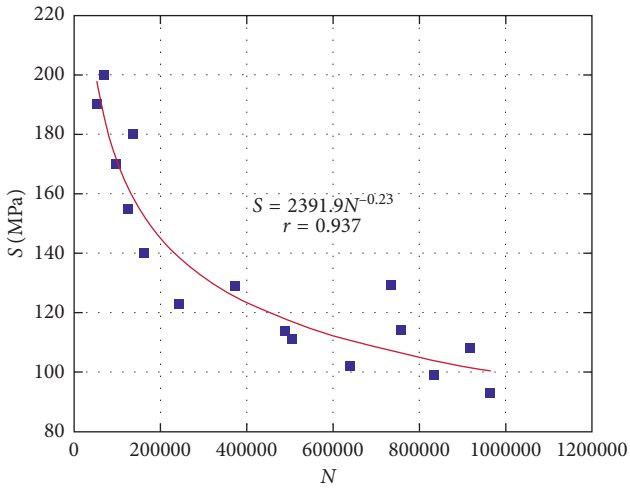

Figure 10: S-N curve.

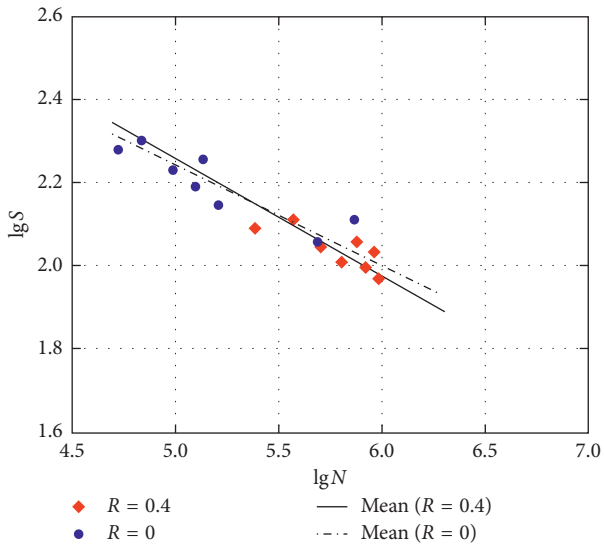

Figure 11: Comparison of lg S-lg N curves with different stress ratios.

$S - 2 \times 0.1557$. When N is equal to 2×10^6, the allowable stress amplitude at the weld toe in the steel tube of WHSJs $[\Delta\sigma]_{2\times10^6}$ is equal to 66.36 MPa, as above aforesaid.

In the Standard for Design of Steel Structures [17], the class Z6 is most similar to WHSJs, but it has a higher allowable stress amplitude ($[\Delta\sigma]_{2\times10^6} = 90$ MPa). We recommend adding the WHSJs as a new type of joint in Standard for Design of Steel Structures.

Yan [19] reported that allowable stress amplitude $[\Delta\sigma]_{2\times10^6}$ is 22 MPa at the weld toe in the hollow sphere of WHSJs under axial force. This value is smaller than 66.36 MPa, which is the allowable stress amplitude of the fatigue failure at the weld toe in the steel tube found in this study. Therefore, the allowable stress amplitudes of two fatigue failure modes of WHSJs should be categorized into two classes.

5. Conclusions

In this paper, the static load and constant-amplitude fatigue tests were carried out on full-scale WHSJs. The constant-amplitude fatigue performance of the weld toe in the steel tube was researched, and the conclusions of this study are as follows:

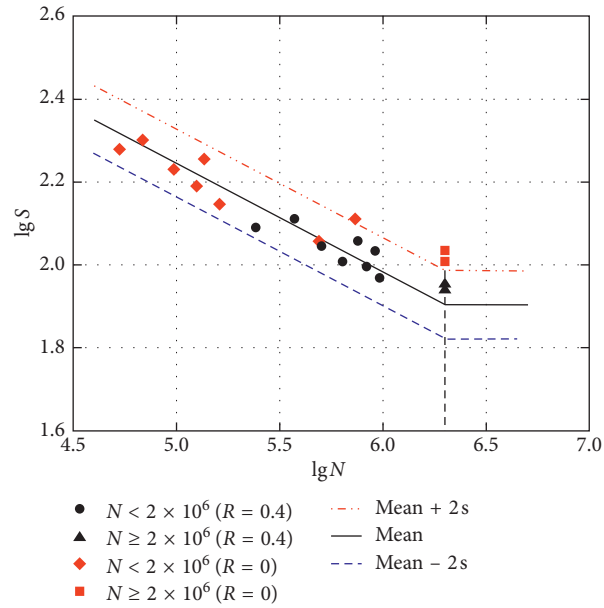

Figure 12: lg S-lg N curve.

(1) The perpendicular stress and parallel stress at the weld toe in the steel tube of WHSJs are both tensile stresses. The parallel stress is about 1/2 of the perpendicular stress. The perpendicular stress and parallel stress at the weld toe in the hollow sphere are also tensile stresses. The stress dropped rapidly at the other positions of the hollow spherical surface that are farther from the weld toe, which indicates that the adjacent members have limited impact on the stress of WHSJ. The maximum stress occurred at the weld toe in the steel tube of the entire joint, where the fatigue failure initiated.

(2) The fatigue failure of the welded joint initiated from the outer surface of the weld toe in the steel tube, and the welding defect was more likely to be the fatigue initiation. The crack propagated from the outside to the inside of the steel tube until it penetrated the steel tube wall.

(3) Twenty effective test data were obtained from the constant-amplitude fatigue test. The stress amplitude was used as a parameter to statistically analyze the data from the fatigue tests with different stress ratios ($R = 0$, 0.4). These data were then fitted to a fatigue curve with double logarithmic coordinates, as shown below:

$$\lg N = 13.5639 - 3.8155 \lg S \pm 2 \times 0.1557. \quad (6)$$

(4) Using the nominal stress amplitude as a parameter, the fatigue design method for the weld toe in the steel tube of WHSJs was established. The nominal stress amplitude is equal to 66.36 MPa while taking

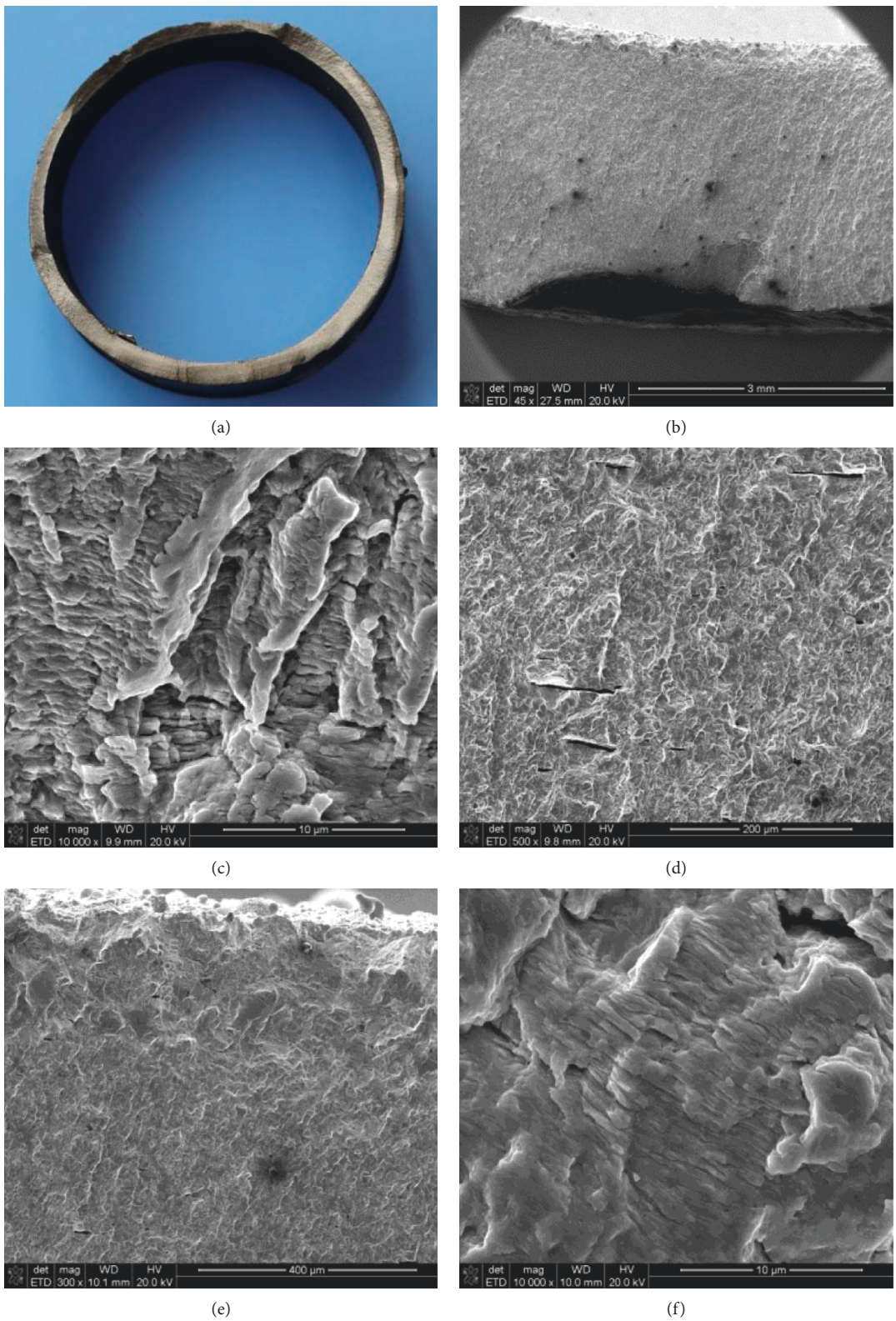

(a) (b) (c) (d) (e) (f)

Figure 13: Typical fracture images (stress amplitude = 123 MPa and stress ratio = 0.4). (a) Macroimage. (b) Micrograph of fatigue initiation zone. (c) Micrograph at 1 mm from the outer wall. (d) Micrograph at 2 mm from the outer wall. (e) Micrograph near the inner wall with 300 times. (f) Micrograph near the inner wall with 10000 times.

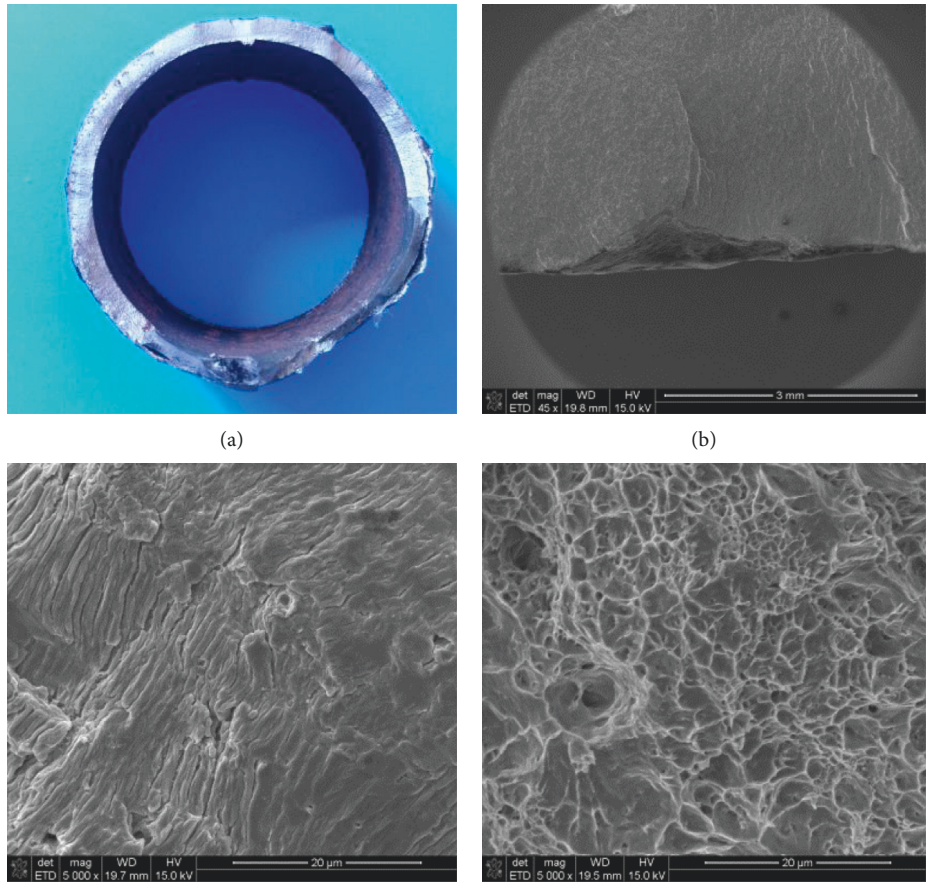

(a) (b) (c) (d)

FIGURE 14: Typical fracture images (stress amplitude = 155 MPa and stress ratio = 0). (a) Macroimage. (b) Micrograph of fatigue initiation zone. (c) Micrograph of fatigue crack propagation zone. (d) Micrograph of fast fracture zone.

$N = 2 \times 10^6$ as the number of cycles. The allowable stress amplitude at the weld toe in the steel tube of WHSJs is lower than the allowable stress amplitude of the class Z6 in Standard for Design of Steel Structures, and the two values cannot be unified. We recommend adding the WHSJs as a new type of joint in the Standard for Design of Steel Structures. The allowable stress amplitude of fatigue failure at the weld toe in the steel tube of WHSJs is larger than that at the weld toe in the hollow sphere, so the allowable stress amplitude of WHSJs should be classified according to the fatigue failure locations.

Data Availability

The data used to support the findings of this study are available from the corresponding author upon request.

Conflicts of Interest

The authors declare that they have no conflicts of interest.

Acknowledgments

The authors would like to thank the National Natural Science Foundation of China for providing financial support (grant no. 51578357).

References

[1] X.-L. Liu, *Design and Construction of Plate Grid Structures*, Press of Tianjin University, Tianjin, China, 2000, in Chinese.

[2] Q.-H. Han and X.-L. Liu, "Ultimate bearing capacity of the welded hollow spherical joints in spatial reticulated structures," *Engineering Structures*, vol. 26, no. 1, pp. 73–82, 2004.

[3] X.-L. Wang and W. Luan, "Ultimate bearing capacity of large-scale welded hollow spherical joint in tests," *Spatial Structures*, vol. 17, no. 3, pp. 43–46, 2011, in Chinese.

[4] S.-L. Dong, H.-J. Tang, and Y. Zhao, "Load-carrying capacity and practical calculation method for welded hollow spherical joints subject to combined axial force and bending moment," *China Civil Engineering Journal*, vol. 38, no. 1, pp. 21–30, 2005, in Chinese.

[5] C.-H. Sun, *Finite Element Analysis of Welded Spherical Joint's Stiffness*, Zhejiang University of Technology, Zhejiang, China, April 2009, in Chinese.

[6] Q. Han, Y. Liu, and Y. Xu, "Stiffness characteristics of joints and influence on the stability of single-layer latticed domes," *Thin-Walled Structures*, vol. 107, pp. 514–525, 2016.
[7] H. Liu, J. Lu, and Z. Chen, "Residual behavior of welded hollow spherical joints after exposure to elevated temperatures," *Journal of Constructional Steel Research*, vol. 137, pp. 102–118, 2017.
[8] J. Lu, H. Liu, and Z. Chen, "Behavior of welded hollow spherical joints after exposure to ISO-834 standard fire," *Journal of Constructional Steel Research*, vol. 140, pp. 108–124, 2018.
[9] Z. Zhao, H. Liu, and B. Liang, "Bending capacity of corroded welded hollow spherical joints," *Thin-Walled Structures*, vol. 127, pp. 523–539, 2018.
[10] H.-G. Lei and D.-Y. Yin, "Research progress on fatigue of grid structure with suspension cranes," *Spatial Structure*, vol. 14, no. 4, pp. 32–36, 2008, in Chinese.
[11] H.-G. Lei, Q. Fu, and X.-J. Liu, "Research progress of steel structure fatigue in past 30 years in China," *Journal of Building Structure*, no. S1, pp. 84–91, 2010, in Chinese.
[12] G.-B. Xu and J. Cui, "Fatigue of space trusses and its fatigue life calculation," *Journal of Building Structure*, no. 2, pp. 25–34, 1994, in Chinese.
[13] JGJ-2010, *Technical Specification for Space Frame Structures*, China Architecture and Building Press, Beijing, China, 2010, in Chinese.
[14] A. Hobbacher, *Recommendations for Fatigue Design of Welded Joints and Components*, Doc. XIII-2151-07/XV-1254-07, International Institute of Welding, Paris, France, 2008.
[15] ANSI/AISC 360-16, *Specification for Structural Steel Building*, American Institute of Steel Construction, Chicago, IL, USA, 2010.
[16] CEN, *Eurocode 3: Design of Steel Structure–Part 1.9: Fatigue*, CEN: European Committee for Standardization, Brussels, Belgium, 2003.
[17] GB50017-2017, *Standard for Design of Steel Structures*, China Architecture and Building Press, Beijing, China, 2018, in Chinese.
[18] H.-G. Lei, "Research on static and fatigue behavior of welded spherical joints in space trusses," *Journal of Building Structure*, vol. 14, no. 1, pp. 2–7, 1993, in Chinese.
[19] Y.-J. Yan, *Theory Analysis and Testing Study on Fatigue Properties of the Steel Tube-Welded Hollow Spherical Joints in Space Latticed Structure*, Taiyuan University of Technology, Taiyuan, China, 2013, in Chinese.
[20] JG/T 11-2009, *Welded Hollow Spherical Node of Space Grid Structures*, China Standard Press, Beijing, China, 2009, in Chinese.